Photosynthesis Research
https://doi.org/10.1007/s11120-017-0476-6

ORIGINAL ARTICLE

Variation in cell size of the diatom *Coscinodiscus granii* influences photosynthetic performance and growth

Dong Yan[1] · **John Beardall**[2] · **Kunshan Gao**[1]

Received: 18 June 2017 / Accepted: 27 December 2017

Abstract
Cell size has implications for the package effect in photon absorption as well as for metabolic scaling of metabolism. In this study, we have avoided species-related differences by using isolates of the marine planktonic diatom *Coscinodiscus granii* with cells of different sizes and grown at different light intensities to investigate their energy allocation strategies. To make full use of incident light, several fold variations in cellular chlorophyll *a* content were employed across cell size. This modulation of pigment-related light absorbance was deemed effective as similar light absorbing capacities were found in all treatments. Unexpected low values of O_2 evolution rate at the highest irradiance level of 450 µmol photons m^{-2} s^{-1} were found in medium and large cells, regardless of more photons being absorbed under these conditions, suggesting the operation of alternative electron flows acting as electron sinks. The growth rate was generally larger at higher irradiance levels except for the large cells, in which growth slowed at 450 µmol photons m^{-2} s^{-1}, suggesting that larger cells achieved a balance between growth and photoprotection by sacrificing growth rate when exposed to high light. Although the ratio of carbon demand to rates of uncatalysed CO_2 diffusion to the cell surface reached around 20 in large cells grown under higher irradiance, the carbon fixation rate was not lowered, due to the presence of a highly effective carbon dioxide concentrating mechanism.

Keywords Diatom · Photosynthesis · Photoacclimation · Photoprotection · Photochemical efficiency of Photosystem I · Cell size

Introduction

The underwater light field is characterized by extreme temporal and spatial variability (Dubinsky and Stambler 2009). Accordingly, phytoplankton may need to acclimate to the highly changing light climate to make better use of the absorbed photons to contribute to or sustain their growth. Acclimation strategies include changing antenna size and/or the number of photosynthetic units to regulate the light capture capacities (Dubinsky and Stambler 2009; Wilhelm et al. 2014). Antenna size can be altered by the modulation of cellular pigment content and composition. Specifically, antenna size is usually increased upon exposure to low irradiance (Dubinsky and Stambler 2009; Fisher and Halsey 2016) and is deceased during high light exposure to minimize photo-damage to the photosynthetic apparatus (Goss and Jakob 2010; Wientjes et al. 2013). Pigment composition can also be altered by the cell as a function of irradiance, and an increase in photo-protectant carotenoids can often be found in high light conditions (Lavaud 2002; Domingues et al. 2012). Under unfavorable conditions such as a sudden exposure to high light, imbalances in the amount of absorbed light and the photosynthetic performance may arise from the existence of alternative electron pathways (Wagner et al. 2006). In diatoms, these pathways include the Mehler reaction, cyclic electron transport around PSI, and electron cycling around PSII (Miyake 2010; Shikanai 2014; Curien et al. 2016; Wagner et al. 2016). These processes can be seen as additional electron sinks for energy dissipation when the non-photochemical dissipation of absorbed energy via linear electron flow might not be able to prevent over-reduction in the photosynthetic apparatus (Vredenberg and Bulychev 2010; Wagner et al. 2016).

Cell size has a large influence on the photophysiology of diatom cells. Firstly, cell size plays a part in affecting light

✉ Kunshan Gao
ksgao@xmu.edu.cn

[1] State Key Laboratory of Marine Environmental Science, Xiamen University, Xiamen, Fujian, China

[2] School of Biological Sciences, Monash University, Clayton, VIC 3800, Australia

Published online: 10 January 2018

absorption (Wilhelm et al. 2014). The absorption properties of densely packed pigments in cells acclimated in low light would be negatively affected by shading and overlapping of pigment molecules, a phenomenon also termed the package effect. For any fixed pigment concentration in a single cell, the chlorophyll *a* (Chl *a*)-specific absorption coefficient of phytoplankton, $a^*(\lambda)$, often decreases with increasing cell size due to a larger optical path length, *d* (Morel and Bricaud 1981; Agustí 1991; Stuart et al. 1998). To counteract this low efficiency, larger cells tend to have lower pigment contents per unit volume to reduce shading due to a dilution effect (Agustí 1991; Fujiki and Taguchi 2002; Finkel et al. 2004). Accordingly, larger cells are believed to be less susceptible to high light exposure because they tend to have lower intracellular pigment concentrations and thus intercept fewer damaging photons per unit pigment than smaller cells (Key et al. 2010). Moreover, considering that smaller cells usually show higher growth and metabolic rates compared to larger cells, cell size could impose a trade-off between high metabolic rates and Photosystem II (PSII) light capture vs susceptibility to PSII photoinactivation, leading to different physiological strategies (Key et al. 2010). Cell size also affects the downstream carbon metabolism to balance light absorption, so as to achieve maximum energy conversion efficiency. Sharpe et al. (2012) reported that larger cells within the diatom species *Ditylum brightwellii* had higher numbers of PSII per unit protein to meet a higher energy requirement compared with smaller cells.

Carbon is usually not considered to be a limiting factor for growth even though it accounts for a large part of phytoplankton biomass. However, at the prevailing seawater pH of approximately 8.1, the concentration of free CO_2 in seawater is only 10–20 µmol L^{-1}, depending on temperature. This value may be lower at the surface of cells due to strong CO_2 assimilation (Wolf-Gladrow and Riebesell 1997; Ploug et al. 1999), especially for larger cells (Kühn and Köhler-Rink 2008; Flynn et al. 2012). Studies have shown that growth rates of larger phytoplankton species were selectively favored by increased dissolved inorganic carbon availability in seawater when compared to smaller-sized species (Burkhardt et al. 1999; Wu et al. 2014), indicating that carbon might be a limiting factor for large cells. As cell size increases, the ratio of surface area to volume decreases (Thingstad et al. 2005), making diffusion increasingly inadequate to meet the cells' demands (Nobel 1999; Litchman et al. 2007). Thick diffusion boundary layers, and hence long diffusion paths, may also exacerbate any carbon shortage, if present.

Coscinodiscus is a genus of large marine-centric diatoms with cell diameters of up to 500 µm (Kühn and Raven 2007). They are usually regarded as among the largest marine planktonic diatom genera (Beardall et al. 2009; Finkel et al. 2010). *C. granii* is a large solitary diatom found in neritic waters and can be easily identified in girdle view due to its wedge-like shape. Although the largest diameter on record of this species is 180 µm (Kraberg et al. 2010), cells with a diameter of 287 µm were observed in the present work. Most studies of effects of size have made comparisons across different species. In this paper, we have attempted to determine how cells of different size (diameter ≈ 120, 200, 280 µm) of *C. granii* make optimal use of absorbed light in response to different light levels. Based on the assumptions above, we hypothesize that, larger cells will tend to be more susceptible to high irradiances considering that a lack of adequate CO_2 supply via diffusion might weaken the impact of the Calvin cycle as an energy sink. Consequently, excess electrons will be diverted into other pathways for dissipation, leading to lower quantum yields of CO_2 assimilation $\left(\Phi_{CO_2}\right)$ as well as lower quantum yields of O_2 evolution $\left(\Phi_{O_2}\right)$ under such conditions.

Materials and methods

Culture conditions

One single cell of *C. granii* with a diameter of 100 µm was isolated from seawater samples of Wuyuan Bay, Xiamen, China in March, 2016. From this single cell, cultures were established and were grown in polycarbonate bottles with filtered (0.45-µm pore size) natural seawater enriched with Aquil nutrients and vitamins (Morel et al. 1979). The incubation irradiances were provided by white LED light (400–750 nm) in an incubator (Ruihua, Wuhan, China) and were set at 70, 125, 225, and 450 µmol photons m^{-2} s^{-1} by either adjusting the distances between bottles and light sources or covering bottles with neutral density filters. All light intensities in this work were measured with a photosynthetically active radiation (PAR) sensor attached to a Multi-Color-PAM (Walz, Effeltrich, Germany). Cultures were maintained at 20 °C with a day/night cycle of 12/12 h. The highest light level set in this experiment corresponds to the highest daily averaged irradiance at the surface seawater in Wuyuan Bay, which was around 450 µmol photons m^{-2} s^{-1}. All cultures were shaken at least 5 times per day and were transferred to new medium every 1 or 2 days to ensure that cells were in their mid-exponential growth phase. Each treatment was carried out with triplicate cultures. The culture inocula were used for optical and photosynthetic measurements after ten generations under the respective conditions.

Cell size and growth

Ten cells of the same size were isolated from a stock culture that had a mixture of diameters ranging from 60 to 287 µm. The large cells in the stock culture were obtained

from the vegetative enlargement of the small cells, as previously reported in *C. wailesii* by Nagai et al. (1995). All cells with almost the same diameter originated from these isolated ten cells. Diameters were recorded during cell counting with Photoshop using pictures taken by a digital camera connected to an inverted microscope (Digital Sight DS-Fi1, Nikon, Japan). The average diameter ($n > 100$) for each treatment during the whole experiment was used for calculations. Cells were approximated to a complex geometrical shape for volume calculation according to Roselli et al. (2013). Cells used in this study were divided into three groups by their average diameters during the incubation period, 120 (113–129, small), 200 (196–214, medium), and 280 (271–287, large) µm. The smallest cells (60 µm) observed were not amenable to culturing for longer than ten generations because they would inevitably change size over this time via the vegetative enlargement process and soon the cell sizes in a single bottle became very heterogeneous. Given that the probability of enlarging increased as they became smaller, the diameter of 120 µm was chosen as the smallest size used in this study.

Cell abundances were counted at least twice daily for each bottle using a plankton chamber under an inverted microscope. The specific growth rate (μ, day^{-1}) was calculated using the following equation:

$$\mu = \frac{\ln(N_t/N_{t-1})}{D_t - D_{t-1}}, \tag{1}$$

where N_t and N_{t-1} are the cell abundance (cells mL^{-1}) at Day t and Day t−1, respectively (Stein 1979).

Chl *a* content and optical absorption coefficient

Cell suspensions were filtered onto GF/F filters with low vacuum pressure (< 0.02 MPa) and soaked in methanol overnight at 4 °C in darkness. The extracts were centrifuged at 6000×*g* for 10 min to remove debris and glass fibers. The absorption spectra from 400 to 800 nm of the supernatant were measured with a spectrophotometer (DU 800, Beckman, USA). The Chl *a* content was calculated according to Ritchie (2006).

The optical absorption coefficient was determined by the quantitative filter technique (Mitchell and Kiefer 1988a, b; Bidigare et al. 1990). Water samples were filtered onto GF/F filters before the immediate recording of the absorption spectra from 400 to 750 nm with a spectrophotometer fitted with an integrating sphere (Lambda950, Perkin-Elmer, USA). A blank filter moistened with filtrate was used as a reference. All absorption spectra were corrected for scattering by subtracting the absorption at 750 nm from the entire spectrum (Mitchell and Kiefer 1988a, b). The optical density obtained from particles in suspension (ODs) was converted from the particles' optical density on the filter (OD_f) according to Cleveland and Weidemann (1993). The Chl *a*-specific absorption coefficient $a^*(\lambda)$ (m^2 mg Chl a^{-1}) was calculated as

$$a^*(\lambda) = \frac{2.3\left[\mathrm{OD_s}(\lambda) - \mathrm{OD_s}(750)\right]}{V/A \cdot \mathrm{Chl}\, a}, \tag{2}$$

where the factor 2.3 converts log to ln, V is the filtered volume, and A is the filtered clearance area of the filter. Chl *a* is the Chl *a* concentration of the cell suspension. The $a^*(\lambda)$ values obtained under different treatments were averaged over the entire visible spectrum from 400 to 700 nm for comparison.

The emission spectra of the light sources used during incubation, oxygen evolution measurements, chlorophyll fluorescence, and P700 measurements were all determined with a fiber optic spectrophotometer (HR4000CG-UV-NIR, Ocean Optics, USA). The photosynthetically absorbed light (Q_{phar}) was calculated according to Gilbert et al. (2000a, b) and Wagner et al. (2006).

Q_a, the dimensionless absorption efficiency factor, is defined as the ratio of energy absorbed within the sphere to the radiant energy impinging on its geometrical cross-section, and expressed as shown in (3) (Morel and Bricaud 1981).

$$Q_a = 1 + \frac{2e^{-\rho'}}{\rho'} + 2 \cdot \frac{e^{-\rho'} - 1}{\rho'^2}. \tag{3}$$

ρ' is the optical thickness due to absorption along the central axis of the cell, assuming cells are spherical, and calculated as

$$\rho' = a_{cm} \cdot d, \tag{4}$$

where a_{cm} is the absorption efficiency factor (m^{-1}) of the cell material and d is the optical path length. a_{cm} is the product of Chl *a* concentration per unit volume and the unpackaged Chl *a*-specific absorption coefficient (Fujiki and Taguchi 2002). The latter was assumed to be 0.025 m^2 mg Chl a^{-1} according to Moisan and Mitchell (1999) and Fujiki and Taguchi (2002).

Q^*_a is the packaging parameter (also known as the specific absorption efficiency) and was calculated according to Morel and Bricaud (1981):

$$Q^*_a = \frac{3}{2} \cdot \frac{Q_a}{\rho'}. \tag{5}$$

Photosynthesis and dark respiration

To investigate the energy conversion efficiencies in the two photosystems, chlorophyll fluorescence and P700 parameters were determined with a Dual-PAM-100 (Walz, Effeltrich,

Germany). In the chlorophyll fluorescence measurement, a series of weak measuring light pulses that induce fluorescence but not photosynthesis is produced. Another set of saturating light pulses is used to briefly suppress the photochemical yield to 0, inducing a maximum fluorescence (F_m) yield from which photosynthesis can be measured. P700 is measured in the dual-wavelength mode (difference of intensities of 875 and 830 nm pulse-modulated measuring light). P700 oxidation is characterized by a positive signal change (Klughammer and Schreiber 2008). Saturation pulses of a photon flux density of 7000 µmol photons m^{-2} s^{-1} and a duration of 400 ms were used in all measurements. The duration time for each light intensity was 30 s to ensure sufficient acclimation time. Since extremely high concentrations of Chl *a* are needed for P700 measurements, cell suspensions buffered with Tris–HCl (20 mmol L^{-1}, pH 8.16) were first concentrated onto GF/F filters with gentle vacuum pressure (< 0.02 MPa) under dim light to make an artificial leaf according to Qiao et al. (2015). The GF/F filter was then immediately used for measurements. In order to obtain the maximum quantum yield of photochemistry in PSII, F_v/F_m, cell suspensions were placed in darkness for at least 8–9 min before filtration. The maximum quantum yield of photochemistry in PSI (YI_{max}) was determined by a saturation pulse in the presence of far-red light. YI and YII are the effective quantum yields of PSI and PSII given by the software.

Oxygen evolution measurements were conducted using a Clarke-type electrode (Hansatech, UK). Cells were harvested by filtering onto mixed cellulose filters (diameter = 25 mm, pore size 8 µm) under gentle vacuum pressure (< 0.02 MPa). The packed cells were resuspended in seawater buffered with 20 mmol L^{-1} Tris–HCl (pH 8.16) with a final Chl *a* concentration of approximately 0.5 µg mL^{-1}. The dark respiration and net oxygen evolution rates at the growth light were determined by covering the cuvette with aluminum foil and adjusting the distances between the light source (white LED) and the cuvette, respectively. The temperature in the water-jacketed cuvette was controlled at 20 °C by a water bath.

For carbon fixation determination, approximately 20 mL of culture was transferred into 24 mL scintillation vials and 100 µL of 5 µCi (0.185 MBq) $NaH^{14}CO_3$ (ICN Radiochemicals, USA) added. The scintillation vials were then placed in the incubator and exposed to the same irradiances and temperature as those in which they were grown for 1 h. After incubation, suspensions were immediately filtered onto GF/F filters with low vacuum pressure (< 0.03 MPa) under dim light. Analyses were conducted according to Helbling et al. (1996) with minor modifications. In short, the filters were exposed to HCl fumes overnight to convert all non-assimilated ^{14}C inorganic carbon into CO_2 and then dried in a thermostatic oven at 60 °C for 5 h. The amount of ^{14}C incorporated by the samples was counted in the presence of 5 mL scintillation cocktail (Hisafe 3, Perkin-Elmer, USA) with a liquid scintillation counter (Tri-Carb 2800TR, Perkin-Elmer, USA). Dissolved inorganic carbon (DIC) was calculated from total alkalinity (TA) and pH by the CO2SYS program (Lewis et al. 1998). TA was measured using the Gran potentiometric titration method according to Anderson et al. (1999).

Carbon demand and supply

The ratio of carbon demand to diffusion via passive influx was calculated to evaluate the carbon shortage in the cell. The diffusion flux to the cell surface (mol s^{-1}) was calculated according to Wolf-Gladrow and Riebesell (1997) and Wu et al. (2014).

$$Q = 4\pi RD\left(1 + R\sqrt{\frac{k'}{D}}\right)\left(\frac{2}{3}[CO_2]_{bulk}\right), \quad (6)$$

where $[CO_2]_{bulk}$ is the dissolved CO_2 concentration in the bulk media given by CO2SYS. With a temperature of 20 °C, S = 35, and pH 8.1, $D = 1.77 \times 10^{-5}$ cm^2 s^{-1}, and $k' = 0.018$ s^{-1} (Wu et al. 2014). R (cm) is the cell radius, which is the half of the optical path length d (cm). The carbon demand (mol s^{-1}) was estimated to be gross carbon fixation rates as given by the liquid scintillation counter.

Statistics

Factorial Analyses of Variance were carried out to test the combined effects of cell size and irradiance. If the treatment impacts were significant, an ANOVA was then performed to check the effect of each individual factor and a post hoc Duncan test was employed. All analyses of variance were conducted after the homogeneity of variance test. For the data that did not satisfy the homogeneity of variance, the treatment effects were examined by Kruskal–Wallis tests. The significance level was 0.05. Origin 9.0 was used for graphing.

Results

Chl *a* content and optical absorption coefficient

Cellular Chl *a* was lower at higher irradiance in all cell sizes (Fig. 1). The highest content was 4.90 ± 0.21 ng $cell^{-1}$ in large cells grown at 70 µmol photons m^{-2} s^{-1}, which was approximately 4 and 6 times higher than that of the medium and small cells under the same light, respectively. When Chl *a* contents were normalized on a volume basis, higher values were found in small cells ($p < 0.01$), followed by 280

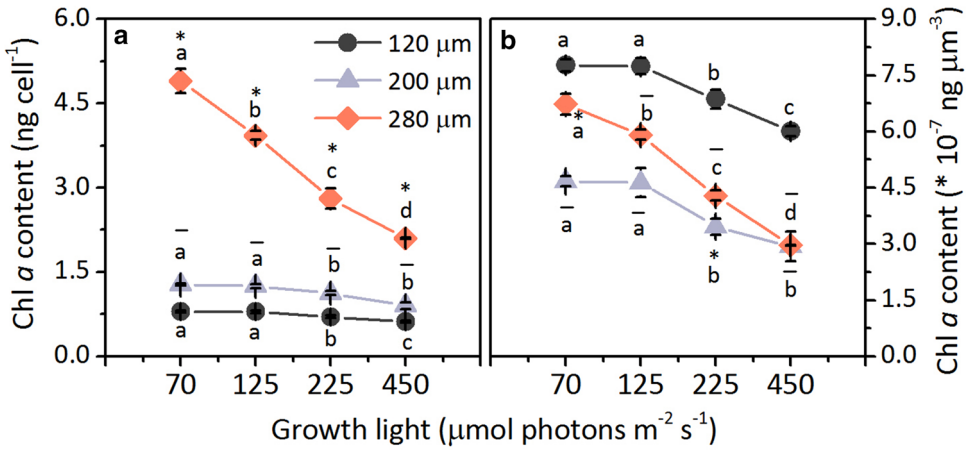

Fig. 1 Chlorophyll *a* (Chl *a*) contents normalized to cell (**a** ng cell^{-1}) or volume (**b** 10^{-7} ng µm^{-3}) in *C. granii* cells. Mean values (±SD) are the average of three independent measurements. Different colors represent different cell sizes. Dark gray circles, 120 µm; light gray triangles, 200 µm; orange diamonds, 280 µm. Different letters indicate significant differences between growth lights. Blank, short horizontal lines and asterisks indicate differences between sizes. ANOVA was performed to check the effect of each individual factor and a post hoc Duncan test was employed. The significance level was 0.05

and/or 200 µm cells at all light intensities. The largest ratio of Chl *a* in cells grown at 70 vs. 450 µmol photons m^{-2} s^{-1} was found in large cells, reaching 2.3, while this ratio was less than 2 for the other two sizes.

Irradiance had a significant effect on the average specific absorption coefficient of Chl *a*, ($\bar{a}^*$) ($p < 0.01$), while for cells with the same size only small cells under 225 µmol photons m^{-2} s^{-1} had a higher value compared with other irradiances ($p < 0.05$) (Table 1). Higher $a^*(440)$ values were found either under 225 or 450 µmol photons m^{-2} s^{-1} in all sizes ($p < 0.05$, Fig. 2). In contrast, $a^*(675)$ did not show much variation. The data for Q_{phar} under growth light showed that medium-sized cells absorbed less light under all irradiances ($p < 0.05$). The maximum Q_{phar} was found in small cells and around 170 µmol photons m^{-2} s^{-1}, which accounts for nearly 40% of the incident irradiance of 450 µmol photons m^{-2} s^{-1}. However, this ratio dropped to 29% in medium-sized cells (Table 1). It also tended to decrease with increasing incident light, suggesting a lower light absorbing efficiency in high light. This trend was in accordance with changes in Q_a (Fig. 3). The range of Q_a values varied with cell size. The largest cells had the largest variability between the lowest and the highest light, around 0.25, indicating a large variation in the light absorbing efficiency, while in small cells this range was only 0.08. Medium-sized cells had the lowest Q_a values under all irradiances ($p < 0.01$ for all light

Table 1 Physiological parameters in different *C. granii* cells exposed to different irradiances

Size (µm)	Growth light (µmol m^{-2} s^{-1})	$\bar{a}^*$ (10^{-3} m^2 mg Chl a^{-1})	F_v/F_m	YI_{max}	Q_{phar} (µmol m^{-2} s^{-1})
120	70	8.62 ± 0.38	0.73 ± 0.00	0.77 ± 0.00	34.26 ± 1.06
	125	8.52 ± 0.47	0.75 ± 0.00	0.71 ± 0.01	60.71 ± 3.65
	225	10.44 ± 1.18	0.70 ± 0.00	0.73 ± 0.03	114.03 ± 9.71
	450	8.13 ± 0.46	0.70 ± 0.00	0.81 ± 0.00	172.69 ± 3.76
200	70	6.94 ± 0.70	0.73 ± 0.00	0.74 ± 0.06	31.77 ± 0.96
	125	9.24 ± 1.26	0.75 ± 0.00	0.75 ± 0.06	60.92 ± 1.65
	225	9.75 ± 1.81	0.75 ± 0.00	0.75 ± 0.02	94.71 ± 3.11
	450	9.48 ± 0.73	0.73 ± 0.01	0.78 ± 0.02	133.30 ± 4.71
280	70	6.44 ± 0.53	0.76 ± 0.01	0.80 ± 0.03	42.82 ± 1.05
	125	6.27 ± 1.46	0.79 ± 0.01	0.78 ± 0.07	69.36 ± 1.85
	225	7.45 ± 0.76	0.75 ± 0.02	0.82 ± 0.03	104.27 ± 3.13
	450	8.41 ± 0.42	0.70 ± 0.03	0.88 ± 0.01	157.32 ± 5.31

Mean values (±SD) of three independent replicates of the averaged light absorption coefficient along photosynthetic active radiation ($\bar{a}^*$), maximum quantum yields of PSII (F_v/F_m) and PSI (YI_{max}) and photosynthetically absorbed irradiance (Q_{phar})

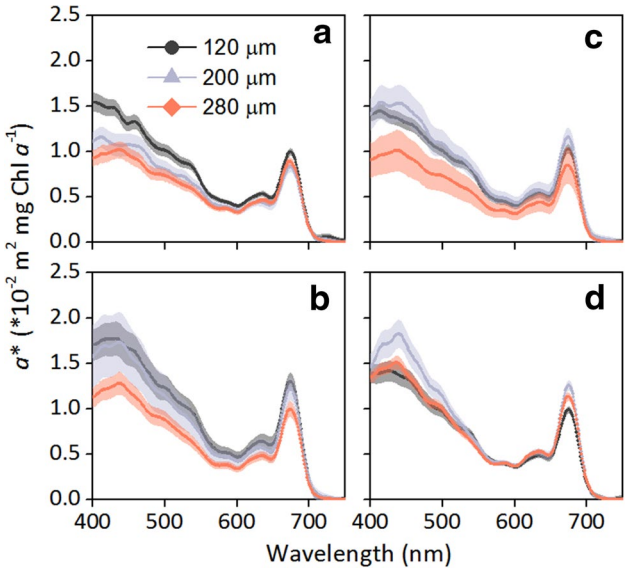

Fig. 2 **a**–**d** are Chlorophyll *a*-specific absorption spectra of cells grown in different light intensities. **a** 70; **b** 125; **c** 225; and **d** 450 µmol photons m^{-2} s^{-1}. Different sizes are represented by lines in different colors. Dark gray circles, 120 µm; light gray triangles, 200 µm; orange diamonds, 280 µm. Mean values (±SD) are the average of three independent measurements. The semi-transparent areas along the line indicate standard deviations

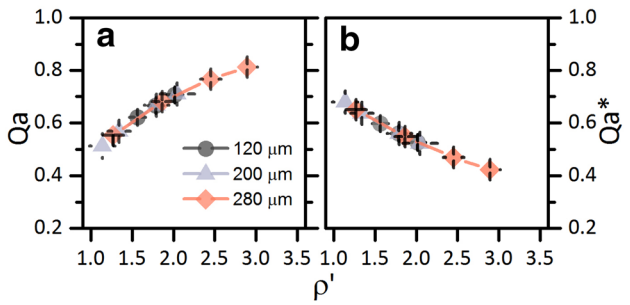

Fig. 3 **a, b** are the absorption efficiency factor (Q_a) and the packaging parameter (Q^*_a) plotted against cellular optical thickness (ρ'). Mean values (±SD) are the average of three independent measurements

intensities). Q^*_a showed similar patterns that the lowest absorption capacity was found under 450 µmol photons m^{-2} s^{-1} ($p < 0.01$).

Photosynthesis

Both the maximum quantum yield F_v/F_m and the effective quantum yield of PSII (YII) decreased with increased light ($p < 0.05$ for F_v/F_m in medium and large cells; $p < 0.01$ for F_v/F_m in small cells; $p < 0.01$ for YII in all sizes) irrespective of cell size (Table 1; Fig. 4). Lower F_v/F_m is usually taken to signify that cells are in poor physiological condition and

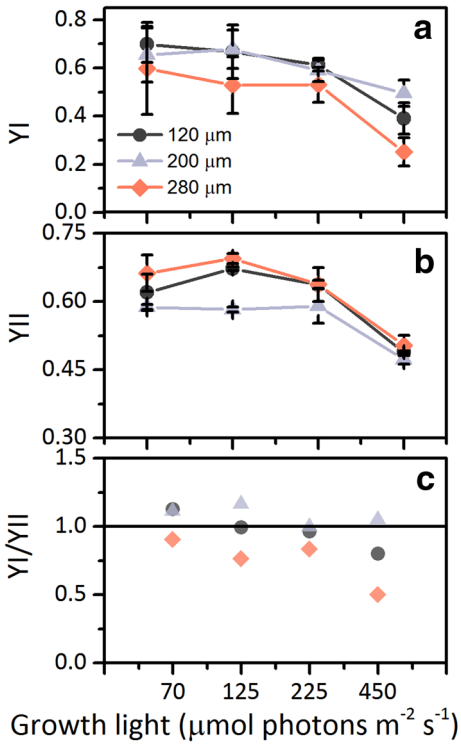

Fig. 4 Photochemical efficiency in the two photosystems measured under growth light. **a** PSI. **b** PSII. **c** Ratios of YI to YII. Mean values (±SD) are the average of three independent measurements. The horizontal line in **c** means that the ratio of YI to YII is 1

that damage might have occurred in PSII. However, even the lowest F_v/F_m (around 0.7) and YII (around 0.5) in this work were relatively high. Therefore, it is hard to judge how these cells were performing from these two parameters, since these values may be favorable when compared with other species. YI_{max} showed no variations except that the value under 70 µmol photons m^{-2} s^{-1} was highest in small cells (Table 1). YI also declined with increased light levels at rates faster than the changes in YII for small and large cells. The rapid decrease in YI resulted in ratios of YI to YII that are less than 1. Maximal values of YI and YII were observed at 70 µmol photons m^{-2} s^{-1} in all size cells, though there were no significant differences for YI due to the large variation in the data. There was a significant decrease in YI and YII in higher light in small and large cells. YI was reduced by around 71% in large cells while the decrease of YII never reached 40% (Fig. 4).

Unexpected low values of O_2 evolution rate (µmol O_2 $cell^{-1}$ h^{-1}) at 450 µmol photons m^{-2} s^{-1} were found in medium and large cells ($p < 0.01$), regardless of the fact that more photons were being absorbed under these conditions (Fig. 5). Unlike O_2 evolution, carbon fixation rates (µmol C $cell^{-1}$ h^{-1}) increased with irradiance. Significantly higher C assimilation rates were found under 450 µmol photons

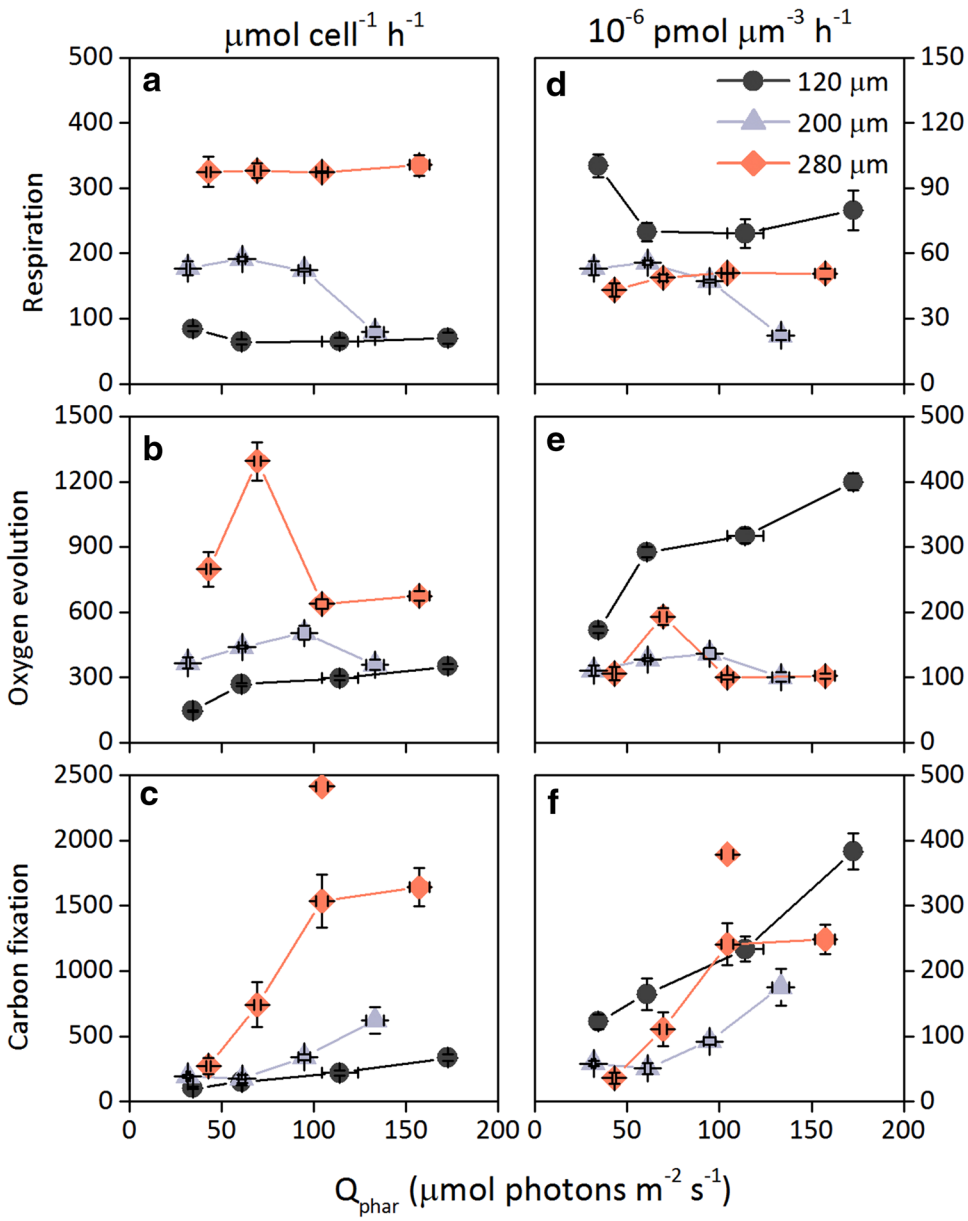

Fig. 5 Oxygen exchange and carbon fixation rates per unit cell or volume as a function of Q_{phar}. **a, d** respiration rate (µmol O_2 $cell^{-1}$ h^{-1} and 10^{-6} pmol O_2 μm^{-3} h^{-1}); **b, e** gross oxygen evolution rate (µmol O_2 $cell^{-1}$ h^{-1} and 10^{-6} pmol O_2 μm^{-3} h^{-1}); **c, f** gross carbon fixation rate (µmol C $cell^{-1}$ h^{-1} and 10^{-6} pmol C μm^{-3} h^{-1}). Mean values (±SD) are the average of three independent measurements except for 280 µm cells grown at 225 µmol photons m^{-2} s^{-1} in **c** and **f**, which was the average of two independent measurements instead of three. One clear outlier was found in **c** and **f** and is shown separately in these figures

m^{-2} s^{-1} for all sizes ($p < 0.05$). Dark respiration rates (µmol O_2 $cell^{-1}$ h^{-1}) for different-sized cells were similar at all light levels except that medium cells had lower rates under 450 µmol photons m^{-2} s^{-1} ($p < 0.01$). Large cells had over three times and nearly one and a half times higher rates than those of small and medium cells grown under lower light intensities, respectively. When the rates were normalized to cell volume, the differences between medium and large cells were not so evident, though small cells showed higher rates.

The discrepancy between oxygen evolution and carbon fixation was also reflected in the quantum yields of O_2 and CO_2 (Fig. 6). Φ_{O_2} and Φ_{CO_2} are defined as the number of moles of O_2 or CO_2 evolved or assimilated, respectively, when 1 mol photons is absorbed. The theoretical value for Φ_{O_2} of 0.125 can only be reached when all absorbed photons are used in photosynthesis, which is not the case under most circumstances. One would expect higher quantum yields under dim light, which is true for O_2 evolution in this work. In all cell sizes, maximum and minimum Φ_{O_2} were found in the lowest and the highest irradiance levels, respectively ($p < 0.05$). In contrast to Φ_{O_2}, the trend was not significant for Φ_{CO_2}, which was indeed higher at 70 µmol photons m^{-2} s^{-1} for small ($p < 0.01$) and medium ($p < 0.01$) cells but greater at 225 µmol photons m^{-2} s^{-1} for large cells ($p < 0.01$). This result suggests that carbon assimilation saturates at much higher irradiances than oxygen evolution and the energy produced in the

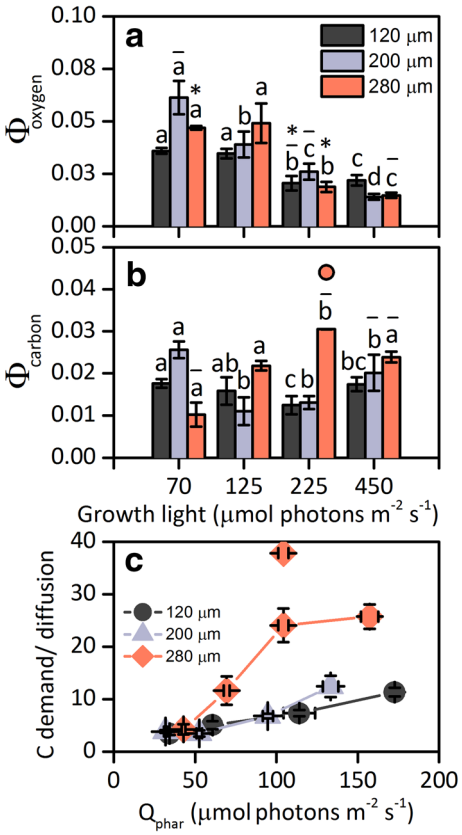

Fig. 6 Quantum yields of O_2 evolution (**a**) and carbon fixation (**b**) in growth light. Φ_{O_2} and Φ_{CO_2} are defined as the number of moles of O_2 or CO_2 evolved or assimilated, respectively, when 1 mol photons is absorbed. **c** The ratio of carbon demand to CO_2 diffusion flux plotted against Q_{phar}. Mean values (±SD) are the average of three independent measurements except for 280 µm cells grown at 225 µmol photons m^{-2} s^{-1} in **c**, which was the average of two independent measurements instead of three. One clear outlier was found in **c** and is shown separately in the figure. Different letters indicate significant differences between irradiances. Blank, short horizontal lines and asterisks indicate differences between sizes. ANOVA was performed to check the effect of each individual factor and a post hoc Duncan test was employed. The significance level was 0.05

light reactions of photosynthesis might not be necessarily enough to support the high energy demand of carbon fixation.

The ratio of carbon demand to diffusion showed an upward tendency with an increase in Q_{phar} (Fig. 6). Much higher ratios, reaching around 20, were found in large cells under 225 and 450 µmol photons m^{-2} s^{-1} ($p < 0.01$), indicating a potential carbon shortage in larger cells given the high carbon fixation rates.

Energy transfer to growth

Growth rates were measured daily during the acclimation period of approximately one week. The growth rates from Day 2 to 7 in the same treatment were averaged for comparison. Cells grew faster in higher incubation irradiances except for the large cells. Large cells grown at 225 µmol photons m^{-2} s^{-1} had the highest growth rate, 0.84 ± 0.02 day $^{-1}$, whereas higher light reduced growth (0.76 ± 0.04 day $^{-1}$) ($p < 0.01$) (Fig. 7). Overall, large cells had longer generation times under all irradiances ($p < 0.05$). The lowest specific growth rate was only 0.51 ± 0.03 day^{-1}, which was nearly threefold lower than the maximum of medium-sized cells grown under 450 µmol photons m^{-2} s^{-1}. Growth rates plotted against Q_{phar} and gross carbon fixation rate per volume showed similar patterns with the largest and smallest slopes found in medium and large cells, respectively.

Discussion

Similar $\bar{a}^*$ values under different irradiances (Table 1) imply a similar light absorbing capacity across different sizes of this species. The narrowest range of absorbed light between the lowest and the highest irradiance levels was around 100 µmol photons m^{-2} s^{-1} in medium-sized cells, which was nearly four times lower than that of the incident light. This suggests that the strategy of antenna size adjustment was to some extent effective. The peak absorption of $a^*(\lambda)$ is generally located at wavelengths of 440 and 675 nm (Culver and Perry 1999). The variability of $a^*(675)$ is mainly caused by Chl *a*, while $a^*(440)$ can be affected by accessory pigments as well (Fujiki and Taguchi 2002). The higher $a^*(440)$ values under high light in this work are probably due to decreased packaging of these accessory pigments. Although cells absorbed more photons under higher incident irradiance, the efficiency of light absorption decreased in spite of less shading. This decrease in Q_a was caused by lower ρ'. ρ' can be seen as the optical thickness due to absorption. When ρ' is infinitely large, reflection does not exist and the absorbing sphere tends to become a perfect black body (Morel and Bricaud 1981). High light resulted in less Chl *a* per volume, making cells more transparent; thus they exhibited lower ρ'. Under the same irradiance level, the Chl *a* content of large cells has to be many fold greater to achieve a similar absorption efficiency when compared to smaller cells due to the longer optical path length. Although large cells had the greatest variability in ρ' values (see Fig. 3), it is likely that they can only benefit from the dilution effect under lower irradiance levels.

The results presented here show most ratios of YI to YII deviated from 1 (see Fig. 4). Therefore, there was a possibility that the activity of CET in the two photosystems was imbalanced. The absolute electron transport rate (ETR) in the two photosystems is usually calculated as ETR_I or ETR_{II} = $Q_{phar} \times 0.5 \times$ YI or YII, where the factor 0.5 assumes that the two photosystems absorb the same amount of light.

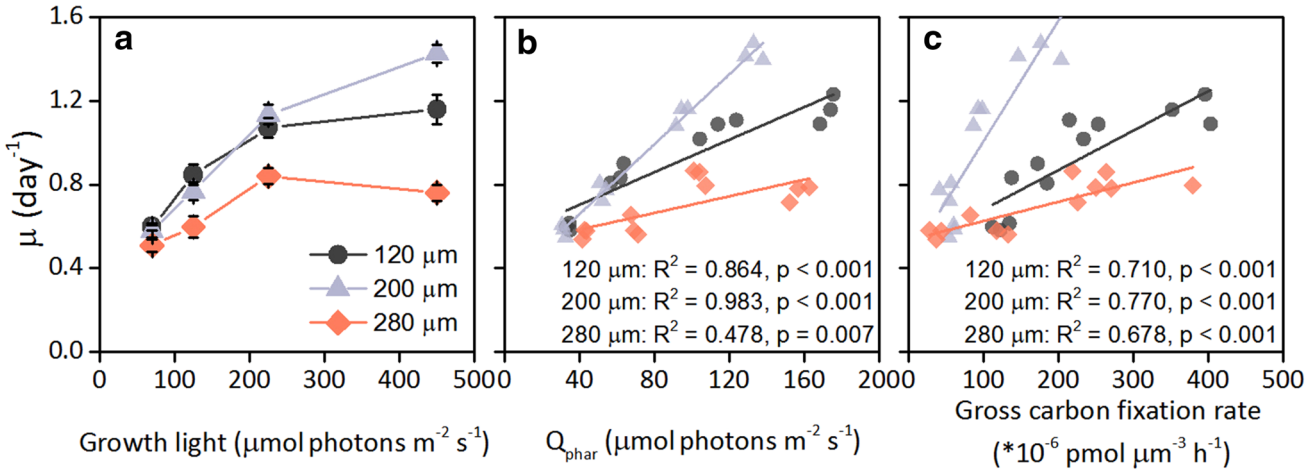

Fig. 7 Averaged specific growth rates plotted against **a** growth light; **b** Q_{phar} and **c** gross carbon fixation rate normalized to cell volume (10^{-6} pmol C μm^{-3} h^{-1}). The solid lines in **b** and **c** are the linear fitted values of growth rate as a function of different independent variables

ETR_{II} should then be the sum of linear electron transport (LET) rate and cyclic electron transport rate in PSII (CET_{PSII}) and ETR_I should be the sum of LET and CET_{PSI}. If YI does not equal to YII, this would reflect CET activity, either in PSI or PSII. Another cause might be the use of the artificial-leaf method in this experiment. Although the filters were kept wet during the measurements, the unnatural conditions could have stressed the cells and made them more sensitive to high light. The quantum yield of PSI depends on the redox states of P700 and the PSI acceptors (Klughammer and Schreiber 2008). The reaction center is open only when P700 is reduced and its acceptor is oxidized. Whether the acceptor side is over-reduced largely depends on the state of carbon fixation since the ultimate electron acceptor of PSI is usually NADP, which is then reduced and used for carbon assimilation as NADPH. Basically, it was unexpected that YI decreased to the extent it did at high irradiances (see Fig. 4) because both the donor and the acceptor side of PSI were not limited, which was reflected by the steady YII and the high carbon assimilation rates. The hypothesis of the "0.5" factor could also be problematic. For optimal performance, the excitation pressure on the two photosystems needs to be balanced (Wientjes et al. 2013). Although no evidence for state transitions has been found in diatoms so far (Cruz et al. 2011; Wilhelm et al. 2014), they can adjust the ratio of PSII to PSI in acclimation to different irradiances (Falkowski et al. 1981). Presumably PSI reaction centers absorbed more light, at least in large cells, whose ratios of YI to YII never exceeded 1 under all irradiances. It is hard to determine which form of CET played a larger part in energy dissipation in this work, and further experiments with modified methodology are necessary to resolve this problem.

The mismatch between the high carbon assimilation rates and the lowered growth rates in large cells grown under high light (see Fig. 7) could result from a larger fraction of the assimilated carbon being excreted either as coating components or as mucilage. Under optimal conditions of light, nutrient availability and temperature, the carbon flux for the synthesis of cell macromolecules is in equilibrium with the energy flux provided by photosynthesis. However, changing environmental conditions can result in a loss of equilibrium between these two fluxes (Wagner et al. 2017). In a study of two different-sized diatom, *Thalassiosira pseudonana* and *T. punctigera*, a prolonged photoperiod, and thus more accumulated photons, was found to be inhibitory to growth of the larger-sized species (Li et al. 2017). The authors proposed that the down-regulation of organic carbon excretion was responsible for the increased carbon fixation per PSII transported electron in shorter photoperiods. The 12-h high light photoperiod in this work, however, might be long enough to cause significant carbon loss through excretion. Diatom frustules are covered externally with organic coatings that may comprise remnants of complex sulphated polysaccharides (Von Stosch 1981). It has been reported that *C. granii* can produce extracellular acidic polysaccharide which contributes to marine mucilage (Fukao et al. 2009). The excretion of mucilage might also contribute to carbon loss based on observations of increased mucilage under higher irradiances (data not shown). Extracellular compounds are supposed to be better able to screen the protoplast than intracellular compounds (Beardall et al. 2009). The release of dissolved organic matter usually increases when exposed to high light (Mueller et al. 2016). It is likely that the excreted carbon plays important roles in photoprotection—either as coating components or as an energy sink.

In the work presented here, the gross oxygen evolution rates either reached a plateau or were reduced under higher irradiances in larger cells, whereas rises in carbon fixation

were observed in high light in cells of all sizes. These data correspond to the variations in Φ_{O_2} and Φ_{CO_2}. Lower quantum yields were found in oxygen evolution but not in carbon assimilation under high light (Fig. 6). When the gross O_2 evolution or the carbon fixation rate is plotted against Q_{phar} (see Fig. 5), one would expect the photosynthetic rates be proportionate to Q_{phar} based on two assumptions. The first is that all absorbed photons lead to release of electrons at PSII and are only involved in the linear electron transport chain (Jakob et al. 2005; Wagner et al. 2006). The second is that carbon assimilation is not limited by its substrate and is the only sink of ATP and redundant produced by the light reaction (Behrenfeld et al. 2008). However, these are not likely to happen in most situations. One possible explanation of the lowered O_2 evolution in larger cells could be that the electrons released in charge separation were dispersed in alternative pathways for energy dissipation. Early findings have provided direct evidence for enhanced oxygen consumption in the light via reduction of O_2 at the PSI acceptor side (Badger et al. 2000), a process termed the Mehler reaction. As one of the water–water cycles, it can act as an electron sink in the dissipation of excess photon energy against photosynthesis (Miyake 2010). The observed low O_2 evolution rates in high light in larger cells might be partly due to the activity of this reaction. However, the O_2 evolution rates of the smallest cells were indeed larger in higher light intensities (see Fig. 6). Hence, we cannot rule out the possibility that cells grown under higher light were more susceptible to damage caused by stirring in the cuvette, especially for larger sizes. When cells were taken out from the cuvette and observed with a microscope after measurements, much more damage was found in cells grown under higher light (data not shown). This might be related to the strength of the frustules. A highly significant inverse relationship between silica content and light intensity has been reported in *C. granii* (Taylor 1985). It is possible that larger diatoms could be more easily damaged by stirring, and reduced mechanical strength of frustules due to the lower silica content in cells grown under higher light further exacerbated the situation. Therefore, the O_2 evolution rate for larger cells grown under high light could have been underestimated.

The high ratios of carbon demand to carbon flux via diffusion (see Fig. 6) suggest a very effective CCM in *C. granii*. Goldman (1999) reported that the active uptake of inorganic carbon ensured free CO_2 was not the limiting factor for growth in *C. granii*. In his work, growth was not limited until pH reached 8.7. The different slopes in both the growth—Q_{phar} and growth—gross carbon fixation plot indicate that the energy utilization efficiencies were lower in large cells while higher in medium-sized cells (see Fig. 7). We suggest that large cells were not necessarily successful in maintaining the balance between growth and photoprotection. Growth was to some extent sacrificed to photoprotection.

This study demonstrated that larger cells were more susceptible to high light stress. Instead of energy being channeled mostly into growth, much energy was allocated to photoprotection. It was surprising that despite the large discrepancy between carbon demand and flux, fixation was light-limited, but not carbon-limited in all cells indicated by similar Φ_{CO_2}. Even if the carbon supply might have been more affected in large cells, the effective CCM ensured a non-substrate limited carbon fixation. The alternative electron transport pathways, such as the Mehler reaction, might have resulted in the lowered net O_2 evolution, though there could be an underestimation of O_2 evolution in medium-sized and large-sized cells. Considering the differential photosynthetic performance among the different sizes of cell, this species could be very competitive when exposed to dynamic changes in coastal environmental conditions.

Acknowledgements The authors would like to thank the two anonymous reviewers for their helpful comments. This study was supported by National Natural Science Foundation (41430967, 41720104005, 41721005), a joint project of National Natural Science Foundation of China and Shandong Province (No. U1606404).

References

Agustí S (1991) Allometric scaling of light absorption and scattering by phytoplankton cells. Can J Fish Aquat Sci 48:763–767. https://doi.org/10.1139/f91-091

Anderson LG, Turner DR, Wedborg M, Dyrssen D (1999) Determination of total alkalinity and total dissolved inorganic carbon. In: Kremling K, Ehrhards M (eds) Methods of seawater analysis. Wiley, Weinheim, pp 127–148

Badger MR, Caemmerer S von, Ruuska S, Nakano H (2000) Electron flow to oxygen in higher plants and algae: rates and control of direct photoreduction (Mehler reaction) and rubisco oxygenase. Philos Trans R Soc B 355:1433–1446. https://doi.org/10.1098/rstb.2000.0704

Beardall J, Allen D, Bragg J et al (2009) Allometry and stoichiometry of unicellular, colonial and multicellular phytoplankton. New Phytol 181:295–309. https://doi.org/10.1111/j.1469-8137.2008.02660.x

Behrenfeld MJ, Halsey KH, Milligan AJ (2008) Evolved physiological responses of phytoplankton to their integrated growth environment. Philos Trans R Soc B 363:2687–2703. https://doi.org/10.1098/rstb.2008.0019

Bidigare RR, Ondrusek ME, Morrow JH, Kiefer DA (1990) In-vivo absorption properties of algal pigments. Proc SPIE Ocean Optics X 1302:290–303. https://doi.org/10.1117/12.21451

Burkhardt S, Zondervan I, Riebesell U (1999) Effect of CO_2 concentration on C:N:P ratio in marine phytoplankton: a species comparison. Limnol Oceanogr 44(3):683–690. https://doi.org/10.4319/lo.1999.44.3.0683

Cleveland JS, Weidemann AD (1993) Quantifying absorption by aquatic particles: a multiple scattering correction for glass-fiber filters. Limnol Oceanogr 38:1321–1327. https://doi.org/10.4319/lo.1993.38.6.1321

Cruz S, Goss R, Wilhelm C et al (2011) Impact of chlororespiration on non-photochemical quenching of chlorophyll fluorescence and on the regulation of the diadinoxanthin cycle in the diatom *Thalassiosira pseudonana*. J Exp Bot 62:509–519. https://doi.org/10.1093/jxb/erq284

Culver ME, Perry MJ (1999) The response of photosynthetic absorption coefficients to irradiance in culture and in tidally mixed estuarine waters. Limnol Oceanogr 44:24–36. https://doi.org/10.4319/lo.1999.44.1.0024

Curien G, Flori S, Villanova V et al (2016) The water to water cycles in microalgae. Plant Cell Physiol 57:1354–1363. https://doi.org/10.1093/pcp/pcw048

Domingues N, Matos AR, Marques da Silva J, Cartaxana P (2012) Response of the diatom *Phaeodactylum tricornutum* to photooxidative stress resulting from high light exposure. PLoS ONE 7:e38162. https://doi.org/10.1371/journal.pone.0038162

Dubinsky Z, Stambler N (2009) Photoacclimation processes in phytoplankton: mechanisms, consequences, and applications. Aquat Microb Ecol 56:163–176. https://doi.org/10.3354/ame01345

Falkowski PG, Owens TG, Ley AC, Mauzerall DC (1981) Effects of growth irradiance levels on the ratio of reaction centers in two species of marine phytoplankton. Plant Physiol 68:969–973

Finkel ZV, Irwin AJ, Schofield O (2004) Resource limitation alters the ¾ size scaling of metabolic rates in phytoplankton. Mar Ecol Prog Ser 273:269–280

Finkel ZV, Beardall J, Flynn KJ et al (2010) Phytoplankton in a changing world: cell size and elemental stoichiometry. J Plankton Res 32:119–137. https://doi.org/10.1093/plankt/fbp098

Fisher NL, Halsey KH (2016) Mechanisms that increase the growth efficiency of diatoms in low light. Photosynth Res 129:183–197. https://doi.org/10.1007/s11120-016-0282-6

Flynn KJ, Blackford JC, Baird ME et al (2012) Changes in pH at the exterior surface of plankton with ocean acidification. Nat Clim Change 2:510–513. https://doi.org/10.1038/nclimate1489

Fujiki T, Taguchi S (2002) Variability in chlorophyll *a* specific absorption coefficient in marine phytoplankton as a function of cell size and irradiance. J Plankton Res 24:859–874. https://doi.org/10.1093/plankt/24.9.859

Fukao T, Kimoto K, Yamatogi T et al (2009) Marine mucilage in Ariake Sound, Japan, is composed of transparent exopolymer particles produced by the diatom *Coscinodiscus granii*. Fish Sci 75:1007–1014. https://doi.org/10.1007/s12562-009-0122-0

Gilbert M, Domin A, Becker A, Wilhelm C (2000a) Estimation of primary productivity by Chlorophyll *a* in vivo fluorescence in freshwater phytoplankton. Photosynth 38:111–126. https://doi.org/10.1023/A:1026708327185

Gilbert M, Wilhelm C, Richter M (2000b) Bio-optical modelling of oxygen evolution using in vivo fluorescence: comparison of measured and calculated photosynthesis/irradiance (P-I) curves in four representative phytoplankton species. J Plant Physiol 157(3):307–314. https://doi.org/10.1016/S0176-1617(00)80052-8

Goldman JC (1999) Inorganic carbon availability and the growth of large marine diatoms. Mar Ecol Prog Ser 180:81–91. https://doi.org/10.3354/meps180081

Goss R, Jakob T (2010) Regulation and function of xanthophyll cycle-dependent photoprotection in algae. Photosynth Res 106:103–122. https://doi.org/10.1007/s11120-010-9536-x

Helbling EW, Chalker BE, Dunlap WC et al (1996) Photoacclimation of Antarctic marine diatoms to solar ultraviolet radiation. J Exp Mar Biol Ecol 204:85–101. https://doi.org/10.1016/0022-0981(96)02591-9

Jakob T, Schreiber U, Kirchesch V et al (2005) Estimation of chlorophyll content and daily primary production of the major algal groups by means of multiwavelength-excitation PAM chlorophyll fluorometry: performance and methodological limits. Photosynth Res 83(3):343–361. https://doi.org/10.1007/s11120-005-1329-2

Key T, McCarthy A, Campbell DA et al (2010) Cell size trade-offs govern light exploitation strategies in marine phytoplankton. Environ Microbiol 12:95–104. https://doi.org/10.1111/j.1462-2920.2009.02046.x

Klughammer C, Schreiber U (2008) Saturation pulse method for assessment of energy conversion in PS I. PAM Appl Notes 1:11–14

Kraberg A, Marcus B, Claus-Dieter D (2010) Coastal phytoplankton: photo guide for Northern European Seas. Pfeil, Munich

Kühn SF, Köhler-Rink S (2008) pH effect on the susceptibility to parasitoid infection in the marine diatom *Coscinodiscus* spp. (Bacillariophyceae). Mar Biol 154:109–116. https://doi.org/10.1007/s00227-008-0904-4

Kühn SF, Raven JA (2007) Photosynthetic oscillation in individual cells of the marine diatom *Coscinodiscus wailesii* (Bacillariophyceae) revealed by microsensor measurements. Photosynth Res 95:37–44. https://doi.org/10.1007/s11120-007-9221-x

Lavaud J (2002) Influence of the diadinoxanthin pool size on photoprotection in the marine planktonic diatom *Phaeodactylum tricornutum*. Plant Physiol 129:1398–1406. https://doi.org/10.1104/pp.002014

Lewis E, Wallace D, Allison LJ (1998) Program developed for CO_2 system calculations. In: Ocean CO_2. http://cdiac.ornl.gov/oceans/co2rprt.html

Li G, Talmy D, Campbell DA (2017) Diatom growth responses to photoperiod and light are predictable from diel reductant generation. J Phycol 53:95–107. https://doi.org/10.1111/jpy.12483

Litchman E, Klausmeier CA, Schofield OM, Falkowski PG (2007) The role of functional traits and trade-offs in structuring phytoplankton communities: scaling from cellular to ecosystem level. Ecol Lett 10:1170–1181. https://doi.org/10.1111/j.1461-0248.2007.01117.x

Mitchell GB, Kiefer DA (1988a) Chlorophyll *a* specific absorption and fluorescence excitation spectra for light-limited phytoplankton. Deep Sea Res A 35:639–663. https://doi.org/10.1016/0198-0149(88)90024-6

Mitchell GB, Kieper DA (1988b) Variability in pigment particulate fluorescence and absorption spectra in the northeastern Pacific Ocean. Deep Sea Res A 35:665–689. https://doi.org/10.1016/0198-0149(88)90025-8

Miyake C (2010) Alternative electron flows (water–water cycle and cyclic electron flow around PSI) in photosynthesis: molecular mechanisms and physiological functions. Plant Cell Physiol 51:1951–1963. https://doi.org/10.1093/pcp/pcq173

Moisan TA, Mitchell BG (1999) Photophysiological acclimation of *Phaeocystis antarctica* Karsten under light limitation. Limnol Oceanogr 44:247–258. https://doi.org/10.4319/lo.1999.44.2.0247

Morel A, Bricaud A (1981) Theoretical results concerning light absorption in a discrete medium, and application to specific absorption of phytoplankton. Deep Sea Res A 28:1375–1393. https://doi.org/10.1016/0198-0149(81)90039-X

Morel FMM, Rueter JG, Anderson DM, Guillard RRL (1979) Aquil: a chemically defined phytoplankton culture medium for trace metal studies. J Phycol 15:135–141. https://doi.org/10.1111/j.1529-8817.1979.tb02976.x

Mueller B, den Haan J, Visser PM et al (2016) Effect of light and nutrient availability on the release of dissolved organic carbon (DOC) by Caribbean turf algae. Sci Rep 6:23248. https://doi.org/10.1038/srep23248

Nagai S, Hori Y, Manabe T, Imai I (1995) Restoration of cell size by vegetative cell enlargement in *Coscinodiscus wailesii* (Bacillariophyceae). Phycologia 34:533–535. https://doi.org/10.2216/i0031-8884-34-6-533.1

Nobel PS (1999) Physicochemical & environmental plant physiology. Academic Press, San Diego

Ploug H, Stolte W, Epping EHG (1999) Diffusive boundary layers, photosynthesis, and respiration of the colony-forming plankton alga. *Phaeocystis* sp. Limnol Oceanogr 44:1949–1958. https://doi.org/10.4319/lo.1999.44.8.1949

Qiao H, Fan X, Xu D et al (2015) Artificial leaf aids analysis of chlorophyll fluorescence and P700 absorbance in studies involving

microalgae. Phycol Res 63:72–76. https://doi.org/10.1111/pre.12073
Ritchie RJ (2006) Consistent sets of spectrophotometric chlorophyll equations for acetone, methanol and ethanol solvents. Photosynth Res 89:27–41. https://doi.org/10.1007/s11120-006-9065-9
Roselli L, Stanca E, Paparella F et al (2013) Determination of *Coscinodiscus* cf. *granii* biovolume by confocal microscopy: comparison of calculation models. J Plankton Res 35:135–145. https://doi.org/10.1093/plankt/fbs069
Sharpe SC, Koester JA, Loebl M et al (2012) Influence of cell size and DNA content on growth rate and photosystem II Function in cryptic species of *Ditylum brightwellii*. PLOS ONE 7:e52916. https://doi.org/10.1371/journal.pone.0052916
Shikanai T (2014) Central role of cyclic electron transport around photosystem I in the regulation of photosynthesis. Curr Opin Biotechnol 26:25–30. https://doi.org/10.1016/j.copbio.2013.08.012
Stein JR (1979) Handbook of phycological methods: culture methods and growth measurements. Cambridge University Press, Cambridge
Stuart V, Sathyendranath S, Platt T et al (1998) Pigments and species composition of natural phytoplankton populations: effect on the absorption spectra. J Plankton Res 20:187–217. https://doi.org/10.1093/plankt/20.2.187
Taylor NJ (1985) Silica incorporation in the diatom *Coscinodiscus granii* as affected by light intensity. Br Phycol J 20:365–374. https://doi.org/10.1080/00071618500650371
Thingstad TF, Øvreås L, Egge JK et al (2005) Use of non-limiting substrates to increase size; a generic strategy to simultaneously optimize uptake and minimize predation in pelagic osmotrophs? Ecol Lett 8:675–682. https://doi.org/10.1111/j.1461-0248.2005.00768.x
Von Stosch HA (1981) Structural and histochemical observations on the organic layers of the diatom cell wall. In: Proceedings of the 6th Diatom Symposium on Recent and Fossil Diatoms. Otto Koetz, Science Publishers, Königstein, pp 231–252
Vredenberg WJ, Bulychev AA (2010) Photoelectrochemical control of the balance between cyclic- and linear electron transport in photosystem I. Algorithm for P700 + induction kinetics. Biochim Biophys Acta BBA 1797:1521–1532. https://doi.org/10.1016/j.bbabio.2010.03.019
Wagner H, Jakob T, Wilhelm C (2006) Balancing the energy flow from captured light to biomass under fluctuating light conditions. New Phytol 169:95–108. https://doi.org/10.1111/j.1469-8137.2005.01550.x
Wagner H, Jakob T, Lavaud J, Wilhelm C (2016) Photosystem II cycle activity and alternative electron transport in the diatom *Phaeodactylum tricornutum* under dynamic light conditions and nitrogen limitation. Photosynth Res 128:151–161. https://doi.org/10.1007/s11120-015-0209-7
Wagner H, Jakob T, Fanesi A, Wilhelm C (2017) Towards an understanding of the molecular regulation of carbon allocation in diatoms: the interaction of energy and carbon allocation. Phil Trans R Soc B 372:20160410. https://doi.org/10.1098/rstb.2016.041
Wientjes E, van Amerongen H, Croce R (2013) LHCII is an antenna of both photosystems after long-term acclimation. Biochim Biophys Acta BBA 1827:420–426. https://doi.org/10.1016/j.bbabio.2012.12.009
Wilhelm C, Jungandreas A, Jakob T, Goss R (2014) Light acclimation in diatoms: from phenomenology to mechanisms. Mar Diatoms 16:5–15. https://doi.org/10.1016/j.margen.2013.12.003
Wolf-Gladrow D, Riebesell U (1997) Diffusion and reactions in the vicinity of plankton: a refined model for inorganic carbon transport. Mar Chem 59:17–34. https://doi.org/10.1016/S0304-4203(97)00069-8
Wu Y, Campbell DA, Irwin AJ et al (2014) Ocean acidification enhances the growth rate of larger diatoms. Limnol Oceanogr 59:1027–1034. https://doi.org/10.4319/lo.2014.59.3.1027